Effect of Na from soda-lime glass substrate and as post-deposition on $Cu(In,Ga)Se_2$ absorbers: A photoelectron spectroscopy study in ultra-high vacuum

I. Majumdar[1,2, a)], V. Parvan[1,3], D. Greiner[1,4], R. Schlatmann[1], I. Lauermann[1,b)]

[1] *PVcomB, Helmholtz-Zentrum Berlin für Materialien und Energie GmbH, Schwarzschildstraße 3, 12489 Berlin, Germany*

[2] *Freie Universität Berlin, Fachbereich Physik, Arnimallee 14, 14195 Berlin, Germany*

[3] *Present address: Feinmetall GmbH, Zeppelinstraße 8, 71083 Herrenberg, Germany*

[4] *Present address: Busch Produktions GmbH, Schauinslandstraße 1, 79689 Maulburg, Germany*

Abstract

Sodium is known to play a crucial role in thin-film solar cells based on $Cu(In,Ga)Se_2$ (CIGSe) absorbers, however, the chemical state of Na in CIGSe is still under discussion. In this work, an Auger parameter analysis has been carried out to identify the differences in the chemical states of Na in CIGSe, originating from two different sources: the soda-lime glass substrate (Na-SLG) and from a post-deposition treatment (Na-PDT). In Na-PDT CIGSe, a Na state with extra positive charges, an In_yO_z phase, a reduced [Cu]/[In] or [Cu]/[Se] ratio at the surface and most favorable formation of Na_{Cu} defects indicates the possible formation of a $(Na_xCu_{1-x})(In_yO_z)$ complex compound. In Na-SLG CIGSe, only Na states possibly located at the grain boundaries at the absorber surface could be identified. Both CIGSe with sputtered Zn(O,S) buffer have been studied to gain an insight on the influence of the absorber surface states on the energy band line-up at the respective absorber/buffer interfaces.

Keywords: $Cu(In,Ga)Se_2$; soda-lime glass; Na post-deposition; Auger parameter; band-alignment

[a)] Email: isheta.majumdar.iitb@gmail.com / isheta.majumdar@helmholtz-berlin.de

[b)] Email: iver.lauermann@helmholtz-berlin.de

1. Introduction

The understanding of the importance of alkali doping began with the research of Hedström et al. [1] in 1993 wherein they investigated Cu(In,Ga)Se_2 (CIGSe) growth on various substrates, one of which included soda-lime float glass that resulted in improved solar cell efficiencies of ~14 %, thus setting a milestone in the development of CIGSe-based solar cell devices. A year later, Holz et al. [2] concluded that the Na from soda-lime glass (SLG) is responsible for the efficiency enhancement in terms of increasing carrier concentration and hence electrical conductivity in the CIGSe layer. After that many different ways of incorporating Na externally into the CIGSe layer were studied, since the Na incorporation from SLG could not be controlled in terms of the amount of Na being incorporated. An overview of all such strategies has been gathered in Salomé et al.'s review paper [3] on incorporation of alkali metals in chalcogenide-based solar cells. One of the last methods to emerge was the so-called "post-deposition treatment" (PDT), which involved depositing ~30 nm of NaF on as-grown CIGSe absorbers [4] that resulted in solar cells as good as the ones using SLG substrates. The same authors investigated the structural effects of Na from SLG and PDT on CIGSe prepared with various substrate temperatures by comparing their device performances [5]. Before Rudmann et al. [4], Lammer et al. [6] had investigated devices made from a Na co-evaporation that involved evaporating elemental Na instead of NaF and compared them to devices using SLG substrates prepared at varying substrate temperatures. Therefore, this has been the motivation behind this work, whereby the structural and electronic effects of Na from SLG and PDT exclusively at the CIGSe surfaces have been studied and compared.

In order to eliminate the toxic CdS buffer layer and its costly preparation process, Zn(O,S) films with freely adjustable [S]/([S]+[O]) (SSO) ratio were prepared by Grimm et al. [7] by reactive sputtering from a ZnS target and the best solar cells were obtained for an SSO composition of 0.25. From band alignment calculations, the results suggested that sputtered ZnS_xO_{1-x} could be used as a substitute for the CdS buffer and the i-ZnO part of the window layer [8]. A detailed band alignment calculation for the CIGSe/ Zn(O,S) interface was done by Pankow et al. [9], where they extracted large conduction band offsets (CBOs), which should normally be detrimental to device performance; but they obtained 18.5 % device efficiencies. They attributed this to thin buffer layers facilitating charge transfer via tunnelling or by defect states. Therefore, in this work, exclusively CIGSe/Zn(O,S) interfaces have been investigated for the CIGSe containing Na from the above mentioned two sources.

2. Material and methods (Experimental)

In this work, an attempt has been made to distinguish (i) Na diffusing from SLG substrate and reaching the CIGSe surface, and (ii) Na incorporated externally by post-deposition of Na metal after CIGSe growth, in terms of chemical changes at the CIGSe absorber surface studied by X-ray Photoelectron Spectroscopy (XPS), as well as electronic changes at the CIGSe absorber surface studied by Ultraviolet Photoelectron Spectroscopy (UPS). The band-alignments at sputtered Zn(O,S)/CIGSe heterojunctions have also been studied for both cases.

For this purpose, surfaces of two types of CIGSe absorbers were studied: (i) CIGSe absorbers grown on a Mo-coated SLG substrate by the standard three-stage co-evaporation process (SI 1), and (ii) Na metal evaporation on CIGSe absorber of type (i) but with an alkali barrier material (SiO_xN_y) deposited before the Mo back contact deposition in order to not allow Na diffusion from SLG. From here on, the CIGSe absorber of type (i) will be called the Na-SLG CIGSe sample and the CIGSe absorber of type (ii) will be called the Na-PDT CIGSe sample for simplicity's sake, even though this alkali treatment is not the same as the conventional PDT, where the post-deposition materials are alkali fluorides in the presence of a Se atmosphere and heated CIGSe substrates and the deposition time being 15-20 minutes, resulting in thick films of thickness of ~10-30 nm. The Na metal deposition for the Na-PDT sample was done in a separate physical vapor deposition (PVD) chamber under ultra-high vacuum (UHV) at the XPS/UPS experimental set-up CISSY (details in SI 3), which is not the same as the CIGSe growth chamber, hence no Se atmosphere. Both the CIGSe absorbers prepared in the CIGSe growth chamber: the Na-SLG CIGSe and the bare CIGSe before Na-PDT, were transferred to the CISSY set-up after a waiting period of ~24 hours, all the while being sealed inside a nitrogen-filled packet. These CIGSe absorbers were exposed to air for the duration of the time that it took to load the samples inside the PVD chamber (~10 minutes). Before loading, the CIGSe absorbers were etched with 5% KCN (aqueous potassium cyanide) solution for three minutes, then washed with deionized water, followed by drying with a nitrogen stream.

For preparation of the Na-PDT CIGSe sample, Na metal in the vapor form was evaporated from a Na dispenser (SI 2) fitted inside the PVD chamber at CISSY with a deposition time of ~2 mins resulting in ~2 nm of Na metal. The Na dispenser is a controllable source of clean Na atomic vapor that is evaporated as a result of a reaction between the mixture of $NaCrO_4$ and reducing/getter agent SAES St 101 (an alloy of 84% Zr and 16% Al) upon Ohmic heating. The action of the getter material is to irreversibly adsorb chemically active gases created during the reduction reaction in order to release clean Na vapor only [10]. The deposited Na metal might not be a completely covered layer but rather an estimate of the amount of Na deposition obtained by depositing Na on a reference Si sample at first (SI 2). This reference sample was

also measured for the Na $1s_{1/2}$ core-level signal and Na KLL Auger line signal and is called the Na-PDT (Si) sample and is treated as the reference sample for the Na-PDT CIGSe sample. Another reference sample for both the Na-SLG CIGSe and Na-PDT CIGSe samples is a CIGSe absorber with an alkali barrier material (SiO_xN_y) but no Na deposition, which is called the Na-free CIGSe sample. None of the samples were subjected to annealing.

For the XPS peak analysis, a linear type background was subtracted for every measured peak. After background subtraction, a measured peak was given a line-shape fitting with a Voigt function, which is a convolution of the Lorentzian and Gaussian functions. All measured peaks were processed using the software PeakFit [11]. All core-level binding energy (BE) values and Auger line kinetic energy (KE) values have been referenced to the Au $4f_{7/2}$ signal of a sputter-cleaned gold foil that has been corrected to a BE position of 84.00 eV as per convention [12].

After XPS/UPS analysis of the Na-SLG CIGSe and Na-PDT CIGSe absorbers in CISSY, the samples were transferred to the sputter chamber of the same setup, thus avoiding intermediate surface contaminations. The Zn(O,S) was RF (radio frequency)-sputtered (13.56 MHz) from a mixed (ZnO, ZnS) target of diameter 125 mm, with an Ar pressure of 5 μbar. The target, with a nominal [ZnS]/([ZnO]+[ZnS]) ratio of 25% [13], was obtained from a commercial supplier. The deposition was carried out with a power density of 1.6 W cm^{-2} at the target surface without deliberate substrate heating.

3. Results and discussion

3.1 Auger parameter analysis of Na chemical states

3.1.1 XPS core-level photoelectron and Auger peaks

The following results are an analysis of the XPS core-level signals Cu $2p_{3/2}$, In $3d_{5/2}$, Ga $2p_{1/2}$, Se $3d_{5/2}$ and Na $1s_{1/2}$ as well as the Auger lines Na $KL_{23}L_{23}$, Cu $L_3M_{45}M_{45}$, In $M_5N_{45}N_{45}$, Ga $L_3M_{45}M_{45}$ and Se $L_3M_{45}M_{45}$ obtained using an Al Kα X-ray source. Figure 1 (a) and (b) show the Na $1s_{1/2}$ photoelectron and Na $KL_{23}L_{23}$ Auger spectra, respectively, measured for the Na-SLG CIGSe, Na-PDT CIGSe samples and the reference sample Na-PDT (Si). Theoretically, the Na $KL_{23}L_{23}$ Auger spectrum for the metal has four components:

$1s\ 2s^2\ 2p^6\ 3s\ {}^1S, {}^3S \rightarrow 1s^2\ 2s^2\ 2p^4\ 3s\ {}^2S$ collectively called $KL_{23}L_{23}$ (^1S);

$1s\ 2s^2\ 2p^6\ 3s\ {}^1S, {}^3S \rightarrow 1s^2\ 2s^2\ 2p^4\ 3s\ {}^2D$ collectively called $KL_{23}L_{23}$ (^1D) [14];

along with several Auger satellite lines due to shake-up of 2p electrons [15] . Table 1 shows all the Na $KL_{23}L_{23}$ Auger spectra peak components obtained in this work.

Table 1 Na $KL_{23}L_{23}$ Auger peak components for Na-PDT (Si), Na-SLG CIGSe and Na-PDT CIGSe.

Samples	**Na-PDT (Si)**		**Na-SLG CIGSe**		**Na-PDT CIGSe**	
Peaks	**KE (eV)**	**% Area**	**KE (eV)**	**% Area**	**KE (eV)**	**% Area**
Na $KL_{23}L_{23}$ (^{1}S)	983.95±0.08	9				
Na $KL_{23}L_{23}$ (^{1}D) (a')	986.88±0.22	17				
Na $KL_{23}L_{23}$ (^{1}D) (a)	988.23±0.07	74	990.25±0.05	100	988.34±0.06	31
Na $KL_{23}L_{23}$ (^{1}D) (b)					989.90±0.16	19
Na $KL_{23}L_{23}$ (^{1}D) (c)					991.59±0.03	50

The experimental Na $KL_{23}L_{23}$ Auger spectrum of Na-PDT (Si) in Figure 1 (b) (top panel) was resolved into the main peak of interest $KL_{23}L_{23}$ (^{1}D) (a) at the highest kinetic energy (KE) side at 988.23±0.07 eV (black bold curve). The peak at the lowest KE side at 983.95±0.08 eV (black dashed curve) was identified to be $KL_{23}L_{23}$ (^{1}S) because of the experimental values of separation between $KL_{23}L_{23}$ (^{1}D) (a) and $KL_{23}L_{23}$ (^{1}S) peaks being 5.0 eV according to [16] and 4.5 eV according to [15] and in this case the separation being 4.28 eV. A third peak in the middle at 986.88±0.22 eV (black dashed curve) was identified to be an Auger satellite peak Na $KL_{23}L_{23}$ (^{1}D) (a') because of the experimental value of separation between Na $KL_{23}L_{23}$ (^{1}D) and the first Auger peak on its lower KE side being 1.35 eV [15].

The experimental Na $KL_{23}L_{23}$ Auger spectrum of Na-SLG CIGSe in Figure 1 (b) (middle panel) is a highly noisy spectrum because the final amount of Na that diffused from the SLG substrate via the CIGSe matrix and accumulated at the surface was very low in quantity as can be seen from the Na $1s_{1/2}$ photoelectron signal intensity of Na-SLG CIGSe (middle panel of Figure 1 (a)) that itself is a noisy spectrum as compared to the Na $1s_{1/2}$ photoelectron signals of Na-PDT (Si) (top panel of Figure 1 (a)) and Na-PDT CIGSe (bottom panel of Figure 1 (a)). Therefore the Na $KL_{23}L_{23}$ Auger spectrum of Na-SLG CIGSe has been fitted with a single Voigt peak instead of a cumulative (envelope) fit of all the components of the reference Na $KL_{23}L_{23}$ Auger spectrum of Na-PDT (Si). The fitting resulted in a peak position of 990.25±0.05 eV. The case of this small signal being fitted with the reference envelope fit is shown in SI 4 along with the associated residual plot. This has been compared with the case of the single Voigt peak fit and the associated residual plot shown in SI 4. It can be seen that the reference envelope fit leaves higher residual intensities (~+150/-250) than the single Voigt peak fit (~+50/-150). It is to be noted that the amount of Na diffusing from the SLG substrate could depend on a number of factors and is a topic of research in itself. To begin with, the

composition and thermal expansion of the SLG substrate could be a deciding factor [17]. Next, the amount of Na accumulated at the Mo surface may determine the amount of Na incorporated into CIGSe [18]. It is known that the oxidization of the Mo layer opens diffusion channels for Na at the Mo/CIGSe interface [19]. The diffusion of Na through the CIGSe then depends on the grain boundary density in CIGSe [20, 21]. Moreover, Na accumulation at the CIGSe surface is directly proportional to the duration of air-exposure of the CIGSe sample [22]. Another CIGSe absorber taken from the same batch in which the currently studied Na-SLG CIGSe absorber was also prepared, was further processed for complete solar cell preparation (standard CdS buffer deposition) that yielded a 14.0 % device efficiency [23].

The experimental Na $KL_{23}L_{23}$ Auger spectrum of Na-PDT CIGSe in Figure 1 (b) (bottom panel) was fitted with the cumulative (envelope) fit of all the components of the reference Na $KL_{23}L_{23}$ Auger spectrum of Na-PDT (Si). The corresponding fitting resolved the spectra into three main peak components: Na $KL_{23}L_{23}$ (^{1}D) (a) at 988.34±0.06 eV, Na $KL_{23}L_{23}$ (^{1}D) (b) at 989.90±0.16 eV and Na $KL_{23}L_{23}$ (^{1}D) (c) at 991.59±0.03. Similar peak components should also be present in the corresponding Na $1s_{1/2}$ photoelectron peak but the fitting software could not resolve the Na $1s_{1/2}$ into three peaks of varying binding energy (BE) positions. So, it is possible that the three components in the photoelectron peak overlap. Moreover, with lab-based X-ray sources, the resolution is not high enough. An alternate fitting of the Na $KL_{23}L_{23}$ Auger spectrum of Na-PDT CIGSe is also possible (SI 5), but owing to the complex nature of Auger spectra it is difficult to conclude which one is the better fit. However, the KE positions of the Na $KL_{23}L_{23}$ (^{1}D) (a) and Na $KL_{23}L_{23}$ (^{1}D) (c) components obtained from the two different fits are quite similar, the differences being 0.18 eV and 0.08 eV, respectively. Considering either of the KE positions leads to the same interpretation of the Na $KL_{23}L_{23}$ (^{1}D) (a) and Na $KL_{23}L_{23}$ (^{1}D) (c) components shown in Section 3.1.3 and thereafter. The fit of Figure 4.1 (b) (bottom panel) has been chosen for further analysis which involves an extra Na $KL_{23}L_{23}$ (^{1}D) (b) component. Measurements were also done with a Mg Kα source and a similar Auger spectrum for Na-PDT CIGSe was observed. A similar Na Auger spectrum was also observed by Song et al. [24] in their NaF-CIGSe depositions.

O $1s_{1/2}$ peaks were measured with a Mg Kα source to avoid the overlap of the Na Auger peak Na $KL_1L_{2,3}$ (^{1}P) (KE 952.63 eV) [15] with the O $1s_{1/2}$ BE region, which would be the case if measured with an Al Kα source.

3.1.2 Auger parameters and Wagner plot

The difference in binding energies between two chemical states depends on both the change in core-electron energy and change in intra-atomic and extra-atomic relaxation energies. In the simplest approximation, for an atom *A*, a chemical shift as a result of two different chemical environments is expressed as [25-27]:

$$\Delta E_B(A) = k\Delta q_A + \Delta V_{MA} + \Delta R^{ea}_A \quad (1)$$

where ($k\Delta q_A + \Delta V_{MA}$) is the initial state effects contribution and ΔR^{ea}_A is the change in extra-atomic relaxation energies in the final state of the photoemission process. V_M and q are the local Madelung potential and the ground state valence charge in the core-ionized atom, respectively. 'k' is an indication of the interactions experienced by the core state as a result of the changes induced in the valence shell of the atom in two different chemical environments.

The modified Auger parameter (α'_A) calculations were done according to the following equation:

$$E_{kin}(KL_1L_{2,3}) = \alpha' - E_B(K) \quad (2)$$

where, α' is called the modified Auger parameter that includes polarisation energy terms needed to stabilize the final state of the Auger emission. Thus, the Auger parameter is the sum of the BE of the photoelectron and the KE of the Auger electron. Such a parameter rules out a possible error from any surface charging effects and is independent of the X-ray source excitation energy.

The *initial state* Auger parameter ($C+2(V_{MA}+kq_A)$) calculations were done according to the following equation:

$$E_{kin}(KL_1L_{2,3}) = [C + 2(V_{MA} + kq_A)] - 3E_B(K) \quad (3)$$

where, the term $[C + 2(V_{MA} + kq_A)]$ is called the *initial state* Auger parameter [28] and is the sum of three times the BE of the photoelectron and the KE of the Auger electron. The quantity 'C' which is a constant is derived from the Hartree-Fock energy of the core electron in the free atom. Both Auger parameter values, α' and $[C + 2(V_{MA} + kq_A)]$ have been tabulated in Table 2.

Compounds with similar final state effects (α'_A=constant) have a linear relationship with slope +1 on the Wagner plot (due to the reverse scale of photoelectron BE). α'_A provides a direct measurement of the extra-atomic relaxation energy, R^{ea}_A due to the total electric field experienced by the ligands, i.e. the one generated by the central positive charge and the one due to induced dipoles on the ligands [29]. On the Wagner plot, the intercept of the line with slope +1 on the ordinate (at E_B=0) gives the value of α'_A. The shifts in this quantity between the different chemical states and the metallic state are the values $2\Delta\alpha'_A$ or the modified

Auger parameter shift, which are approximately $2\Delta R^{ea}_{A}$ in the simplistic electrostatic model [26]. Compounds with similar initial state effects ($C+V_{MA}+kq_A$=constant) have a linear relationship with slope +3 on the Wagner plot, i.e. the sum of the site potential V_{MA} or Madelung potential (from surrounding atoms) and local valence charge on the atom q_A is a constant. On the Wagner plot, the intercept of the line with slope +3 on the ordinate (at E_B=0) gives the value of $C+2(V_{MA}+kq_A)$. The shifts in this quantity between the different chemical states and the metallic state are the values $2\Delta(V_{MA}+kq_A)$ or the *initial state* Auger parameter shift, where C being a constant value for the free atom is not in the expression.

Figure 2 is a Wagner plot of Na compounds. The photoelectron BEs are plotted in the negative x-axis and the Auger KEs are plotted in the y-axis. The +1 slope intercepts or the modified Auger parameters (α'_{Na}) are also shown on the plot. The intention of the experiments was to be able to deposit clean metallic Na on Si substrate, however, that was not the case as the presence of O and C were detected along with Na in XPS measurements. Na vapor is highly reactive; the presence of even small traces of most elements will result in some form of chemical reactions. Hence, the reference Na-PDT (Si) sample is not pure metallic Na. The position of metallic Na has not been shown in the Wagner plot of Figure 2 as its position on the plot is at the extreme far left corner (i.e. at the highest photoelectron BE and highest Auger electron KE) and its inclusion in the plot would have clustered the rest of the compounds position at a confined spot and made them indistinguishable.

Table 2 All elemental core-level photoelectron BE, Auger electron KE and modified and *initial state* Auger parameter values obtained for Na-SLG CIGSe, Na-PDT CIGSe, Na-free CIGSe and Na-PDT (Si).

CIGSe Samples	**Photoelectron BE (eV)**	**Auger electron KE (eV)**	**Modified Auger parameter (eV)**	***Initial state* Auger parameter (eV)**
	Na $1s_{1/2}$	**Na $KL_{23}L_{23}$**	**α'_{Na}**	**C+2(V_{MNa}+kq_{Na})**
Metallic Na [30]	1071.50±0.10	994.20±0.10	2065.70±0.14	4208.70±0.32
Na-PDT (Si)	1072.18±0.01	988.23±0.07	2060.41±0.07	4204.77±0.08
Na-SLG	1071.61±0.01	990.25±0.05	2061.86±0.05	4205.08±0.06
Na-PDT (a)	1072.06±0.01	988.34±0.06 (a)	2060.40±0.06	4204.52±0.07
Na-PDT (b)	1072.06±0.01	989.90±0.16 (b)	2061.96±0.16	4206.08±0.16
Na-PDT (c)	1072.06±0.01	991.59±0.03 (c)	2063.65±0.03	4207.77±0.04
	Cu $2p_{3/2}$	**Cu $L_3M_{45}M_{45}$**	**α'_{Cu}**	**C+2(V_{MCu}+kq_{Cu})**
Metallic Cu [31]	932.80±0.10	918.50±0.10	1851.30±0.14	3716.90±0.32
Na-free	931.88±0.01	917.44±0.05	1849.32±0.05	3713.08±0.06
Na-SLG	932.02±0.01	917.25±0.03	1849.27±0.03	3713.31±0.04
Na-PDT	932.45±0.01	917.07±0.03	1849.52±0.03	3714.42±0.04
	In $3d_{5/2}$	**In $M_5N_{45}N_{45}$**	**α'_{In}**	**C+2(V_{MIn}+kq_{In})**
Metallic In [32]	443.40±0.10	403.90±0.10	847.30±0.14	1734.10±0.32
Na-free	444.48±0.01	400.84±0.04	845.32±0.04	1734.28±0.05
Na-SLG	444.61±0.01	400.65±0.10	845.26±0.10	1734.48±0.10
Na-PDT	444.62±0.01	400.54±0.06	845.16±0.06	1734.40±0.07
	Ga $2p_{3/2}$	**Ga $L_3M_{45}M_{45}$**	**α'_{Ga}**	**C+2(V_{MGa}+kq_{Ga})**
Metallic Ga [33]	1116.30±0.10	1068.30±0.10	2184.60±0.14	4417.20±0.32
Na-free	1117.48±0.01	1065.68±0.08	2183.16±0.08	4418.12±0.08
Na-SLG	1117.78±0.01	1065.60±0.06	2183.38±0.06	4418.94±0.07
Na-PDT	1117.76±0.01	1065.32±0.12	2183.08±0.12	4418.60±0.12
	Se $3d_{5/2}$	**Se $L_3M_{45}M_{45}$**	**α'_{Se}**	**C+2(V_{MSe}+kq_{Se})**
Metallic Se [34]	55.70±0.10	1306.70±0.10	1362.40±0.14	1473.80±0.32
Na-free	53.92±0.01	1307.21±0.01	1361.13±0.01	1468.97±0.03
Na-SLG	54.10±0.01	1307.12±0.02	1361.22±0.02	1469.42±0.04
Na-PDT	54.18±0.01	1306.79±0.01	1360.97±0.01	1469.33±0.03

3.1.3 Separation of initial and final state contributions

In order to separate initial and final state contributions using the two types of Auger parameter shifts, the $\Delta(V_{MA}+kq_A)$ and $\Delta R^{ea}{}_A$ values have been calculated for all elemental components relative to the respective metallic state values. This is represented graphically in Figure 3, which shows a plot of the initial state ($\Delta(V_{MA}+kq_A)$) and the final state ($-\Delta R^{ea}{}_A$) contributions for all elements involved. The $-\Delta R^{ea}{}_A$ values (red bars) have been plotted (on the positive x-scale) to separately show their variation from the $\Delta(V_{MA}+kq_A)$ (grey bars) values. Shorter red bars compared to the reference Na-PDT (Si) or Na-free component red bars imply less negative $\Delta R^{ea}{}_A$ values, i.e. higher relaxation energies as compared to the Na-PDT (Si) or Na-free components. This actually implies higher polarizabilities of the attached ligands. Shorter grey bars compared to reference Na-PDT (Si) or Na-free component grey bars for $\Delta(V_{MA}+kq_A)$ values imply more positive charge or decreased electron density [35] as compared to the Na-PDT (Si) or Na-free components. Among all elements, it seems that considering the error margins, BE shifts in only the Na components (w.r.t their respective metallic states) are majorly affected by the final state relaxation of the core hole. Cu and Ga component shifts seem to be affected majorly by initial state effects, i.e. contribution from initial charge and/or local Madelung potential from surrounding atoms. Within the error margins there are no changes in Auger parameters for In and Se.

3.1.4 Na speciation

From Figure 3, it can be seen that within the error margins, the Na-PDT (a) component of Na has the same initial and final state effects as the reference Na-PDT (Si) component. In the Wagner plot of Na shown in Figure 2 as well, these two components lie on the same slope. Therefore, the Na-PDT (a) component of Na in Na-PDT CIGSe is basically the state in which the Na is evaporated from the Na dispenser. Therefore, this component is called the as-deposited Na state and could be some oxidized form of Na.

Looking at the Wagner plot of Figure 2, the Na-PDT (b) component of Na lies along a line with compounds like NaCl and Na_2SeO_3 that indicate bonding with highly polarizable anions and high coordination number. It can be further seen that the Na-SLG component of Na also lies within the error margin of the Na-PDT (b) component. Both these components also have higher relaxation energies (red bars). This could mean that such components are in close proximity to polarizable anions. These could be attributed to Na in grain boundaries as are known to be present in the CIGSe grain boundaries for Na from SLG [36]. These could be the grain boundaries that open up at the CIGSe surface. It should be noted that the formal oxidation numbers of Cu, In, Ga, Se and Na in all the sample surfaces are +1, +3, +3, -2 and +1, respectively,

From Figure 3 it can be seen that the Na-PDT (b) component of Na shows a positive $\Delta(V_{MNa}+kq_{Na})$ change (grey bars) w.r.t the reference Na-PDT (Si) component. However, there are no complementary changes i.e. negative $\Delta(V_{MA}+kq_{A})$ values seen in any of the CIGSe-related components. This means the Na-PDT (b) component of Na has a reduced local electron density or extra positive charge. Within the error margins, the Na-SLG component of Na shows no $\Delta(V_{MNa}+kq_{Na})$ change. But there is a slight positive $\Delta(V_{MGa}+kq_{Ga})$ change in the Na-SLG component of Ga. This means the Na-SLG component of Ga has a reduced local electron density or an extra positive charge.

From Figure 3 it can be seen that among all the Na-PDT components of Na, Na-PDT (c) seems to have the largest positive ΔR^{ea}_{Na} change as well as the most influenced by initial state effects indicated by the largest positive $\Delta(V_{MNa}+kq_{Na})$ change w.r.t the reference Na-PDT (Si) component. This indicates a positive potential due to withdrawal of electrons by highly polarizable surrounding ligands [35] as well as a high coordination number. Heske et al. [37] had suggested the formation of a Na-O-CIGSe complex at room temperature. This Na-PDT (c) component of Na can therefore be attributed to electron contribution for the formation of a similar Na-containing complex compound at the Na-PDT CIGSe surface.

A positive $\Delta(V_{MCu}+kq_{Cu})$ change is also seen in the Na-PDT component of Cu. This means these components have largely reduced local electron densities and are hence highly polarizable. Parvan et al. [38] have also observed an increase in BE of Cu $2p_{3/2}$ after Na metal deposition, which they have also attributed to reduced electron density in Cu. A Cu depletion at the Na-PDT CIGSe surface is also seen from surface composition calculations ([Cu]/[In] and [Cu]/[Se] ratios) obtained from XPS quantitative analysis, shown in Table 3. Quantitative analysis of the XPS measurements was done by converting the raw data into normalized peak intensities by dividing the peak areas by the following factors: the number of scans (N), the IMFP (λ) of ejected photoelectrons which is a measure of the average distance travelled by an electron beam through a material before it loses energy through inelastic scattering and its intensity is reduced to a fraction of 1/e of the initial intensity, the photoionization cross-sections of emitted photoelectrons (σ) [39] and the transmission function of the spectrometer (T). According to Malitckaya et al.'s theoretical paper [40], Na_{Cu} is the most stable state defect that can form.

Table 3 Surface composition from XPS quantitative analysis.

Samples	[Cu]/[In]	[Cu]/[Se]
Na-free	0.50	0.45
Na-SLG	0.50	0.43
Na-PDT	0.44	0.34

A change in the BE position in the O $1s_{1/2}$ peak in Na-PDT CIGSe relative to the Na-free CIGSe can be an indication of the changed state of oxygen due to the above mentioned Na-containing complex compound formation (SI 6).

Although Auger parameters of In components do not seem to differ significantly, the In $M_{4,5}N_{45}N_{45}$ Auger peaks measured for the samples (Figure 4) show a significant change in the shoulder of the In $M_5N_{45}N_{45}$ Auger peak (most intense peak on the lower KE side) as well as in the shoulder of the In $M_4N_{45}N_{45}$ Auger peak (most intense peak on the higher KE side) in the In component of Na-PDT CIGSe. This indicates the possible formation of a thin In_yO_z containing layer which can possibly be part of the above mentioned Na-containing complex compound. The role of the In atoms in the case of a Na-O-CIGSe complex formation has also been indicated by Heske et al. [37].

Thus, the Na-PDT (c) component of Na maybe part of a complex compound in the surrounding of highly polarizable ligands in the form of reduced electron density in Cu and which also involves Na replacing Cu and an In_yO_z containing surface layer being part of the complex. Therefore, the complex compound itself could be of the form $(Na_xCu_{1-x})(In_yO_z)$. It would be insightful to calculate the formation enthalpy of such a compound using first-principles Density Functional Theory (DFT), but it is out of the scope of this study. Theoretically, the possibility of the formation of a $NaInSe_2$ secondary phase was predicted by Wei et al. [41] because of the high negative formation enthalpy (-3.9 eV) of this compound. However, in our studies of the Na-PDT CIGSe absorber surface, XPS measurements showed no change in the Se environment (seen in Figure 3) that would indicate such a phase formation upon Na deposition. Moreover, $NaInSe_2$ is supposed to be a high band-gap compound (theoretical band gap of 2.16 eV [40]). But valence band maximum (VBM) position measurement (shown in Figure 5 of the next section) of the Na-PDT CIGSe absorber surface also does not indicate a wide band-gap surface phase formation.

Table 4 summarizes all the Na-components identified at the Na-SLG CIGSe and Na-PDT CIGSe surfaces with the help of Auger parameter analysis.

Table 4 Components at Na-SLG CIGSe and Na-PDT CIGSe absorber surfaces.

Na-SLG CIGSe	**Na-PDT CIGSe**
✓ Grain boundary Na states ✓ Ga states with extra positive charges	✓ As-deposited Na states ✓ Grain boundary Na states with extra positive charges ✓ Na-containing complex: $(Na_xCu_{1-x})(In_yO_z)$

3.2 Effect of Na on the Cu(In,Ga)Se_2/Zn(O,S) interface

Studying the band-alignment of the Na-SLG CIGSe and the Na-PDT CIGSe absorber surfaces with an in-system, sputter-deposited Zn(O,S) layer (in-contrast to wet-chemically deposited CdS buffers) was chosen in order to avoid a break in vacuum and enable instantaneous XPS/UPS measurements after Zn(O,S) sputter-deposition onto the Na-SLG CIGSe and Na-PDT CIGSe samples. An initial ultra-thin layer deposition of 10 s of Zn(O,S) deposition time was followed by a final thick layer deposition of approximately 90 s of Zn(O,S) deposition time on both CIGSe samples. XPS core-level measurements for the CIGSe absorber surfaces and Zn(O,S) buffer layers were done using the Mg Kα X-ray source. The initial ultra-thin layer deposition was such that it allowed XPS core-level measurements from both the overlayer Zn(O,S) as well as the CIGSe surface below it. The final thick layer deposition was such that only the overlayer Zn(O,S) core-level XPS signals were attainable and no signal for the underlying CIGSe surface could be observed. So the thickness of this layer can be approximated to be at least 10 nm, which is the average information depth for lab-based XPS measurements. The core-level BE positions were used to obtain the interface-induced band-bending effects in the junction formation.

The current procedure of band-alignment calculation has been adapted from [9]. The valence band offset (VBO) and the conduction band offset (CBO) energy values were calculated as:

$$\Delta E_{VBO} = [E_{CL}^{Zn(O,S)} - E_{VB}^{Zn(O,S)}] - [E_{CL}^{CIGSe} - E_{VB}^{CIGSe}] - \Delta E_{CL} \quad (4)$$

$$\Delta E_{CBO} = [E_g^{Zn(O,S)} - E_g^{CIGSe}] + \Delta E_{VBO} \quad (5)$$

where $E_{CL}^{Zn(O,S)}$ is the core-level BE position of Zn $2p_{3/2}$ line in the final thick Zn(O,S) layer, $E_{VB}^{Zn(O,S)}$ is the valence band maximum (VBM) position for the final thick Zn(O,S) layer, E_{CL}^{CIGSe} is the core-level BE position of the In $3d_{5/2}$ line in the CIGSe absorber before Zn(O,S) deposition, E_{VB}^{CIGSe} is the VBM position for the CIGSe absorber before Zn(O,S) deposition in Equation (4). $E_g^{Zn(O,S)}$ and E_g^{CIGSe} in Equation (5) are the band gap (E_g) values of the final thick Zn(O,S) layer and the CIGSe absorber before Zn(O,S) deposition. ΔE_{CL} is the core-level energy difference between the Zn $2p_{3/2}$ line BE position from the initial ultra-thin Zn(O,S) overlayer and In $3d_{5/2}$ line BE position from the CIGSe surface below it. This is the correction factor for interface-induced band-bending at the absorber/buffer interface region.

The VBM positions (relative to E_F=0 eV) for Na-SLG CIGSe and Na-PDT CIGSe absorbers were measured using UPS with a He I source (21.22 eV) as shown in Figure 5. The method of determination of the VBM position has been explained in SI 7. The VBM at the reference Na-free CIGSe absorber surface has been measured to be 0.62±0.06 eV. It is to be noted that extrapolation of the last linear portion of the VB spectrum of the Na-PDT CIGSe absorber surface (blue dashed lines in Figure 5) would result in negative values of

VBM which is physically meaningless. Therefore, this linear portion has not been considered for the VBM determination. However, such a feature on the VB spectrum is usually an indicator of a surface species formation [42]. Nevertheless, from the VBM determination approach considered in this work, it has been found that the Na-PDT CIGSe absorber surface has a reduced VBM at 0.48±0.06 eV compared to the Na-free CIGSe VBM value. This could indicate enhanced p-type doping at the Na-PDT CIGSe surface. On the other hand, the Na-SLG CIGSe absorber surface has an increased VBM value at 0.87±0.06 eV and hence reduced p-type doping at the surface. A decrease in VBM in Na-PDT CIGSe may also indicate reduced band-bending at the surface and this has also been observed by Rau et al. [43]. From UPS measurements (SI 8), it has been also observed that there is a significant reduction in work function (ϕ) at the Na-PDT CIGSe surface (ϕ=3.24±0.04 eV) as compared to the Na-SLG CIGSe surface (ϕ=4.23±0.06 eV) and Na-free CIGSe surface (ϕ=4.66±0.04 eV).

The ΔE_{VBO} values were calculated using the above attained VBM values for the two CIGSe absorbers before Zn(O,S) deposition as well as the VBM values for the final thick Zn(O,S) layer deposited on both CIGSe absorbers whose values have been shown in Table 5 along with their core-level BE positions and ΔE_{CL} values at the Zn(O,S)/CIGSe interface (initial ultra-thin Zn(O,S) deposition) for the two absorbers.

Table 5 VBO calculation of the Na-SLG CIGSe/Zn(O,S) and Na-PDT CIGSe/Zn(O,S) interfaces.

Sample	**$E_{CL}^{Zn(O,S)}$**	**E_{CL}^{CIGSe}**	**$E_{VB}^{Zn(O,S)}$ (eV)**	**E_{VB}^{CIGSe} (eV)**	**ΔE_{CL} (eV)**		**ΔE_{VBO}(eV)**
	Zn $2p_{3/2}$ (eV)	**In $3d_{5/2}$ (eV)**			**Zn $2p_{3/2}$ (eV)**	**In $3d_{5/2}$ (eV)**	
Zn(O,S)/Na-SLG	1021.84±0.01	444.50±0.01	1.99±0.05	0.87±0.06	1021.99±0.01	444.84±0.01	-0.93±0.08
					577.15±0.01		
Zn(O,S)/Na-PDT	1022.06±0.01	444.56±0.01	1.95±0.06	0.48±0.06	1021.96±0.01	444.73±0.01	-1.20±0.09
					577.23±0.01		

E_g^{CIGSe} values for both Na-SLG CIGSe and Na-PDT CIGSe absorbers were calculated from the [Cu]/([In]+[Ga]) (CGI) and [Ga]/([In]+[Ga]) (GGI) ratios in the two absorbers obtained from quantitative XPS analysis. It is known that the Cu content affects the surface band gap through the formation of Cu-poor defect chalcopyrite phases like $Cu(In_{1-x}Ga_x)_3Se_5$, which is an ordered defect compound (ODC) [44]. Hence, surface band-gaps are typically larger than their bulk values of ~1.1 eV [45] and are relevant for band-alignment calculations. So, E_g values for both CIGSe samples were estimated as [9]:

$$E_g^{CIGSe} = 1.5 \cdot (Eg^{112} - Eg^{135}) \cdot [Cu]/[(In+Ga)] + 1.5 \cdot Eg^{135} - 0.5 \cdot Eg^{112} \quad (6)$$

where, Eg^{112} is the band gap of the $Cu(In_{1-x}Ga_x)Se_2$ phase and Eg^{135} is the band gap of the $Cu(In_{1-x}Ga_x)_3Se_5$ phase. E_g^{112} values have been calculated as [46]:

$$E_g^{112} = 1.01 + 0.626 \cdot x - 0.167 \cdot x \cdot (1-x) \quad (7)$$

whereas, E_g^{135} values have been calculated as [44]:

$$E_g^{135} = 1.193 + 0.415 \cdot x + 0.24 \cdot x^2 \quad (8)$$

where, x = [Ga]/[(In+Ga)] values were obtained from quantitative XPS analysis.

$E_g^{Zn(O,S)}$ values for the Zn(O,S) deposition on both Na-SLG CIGSe and Na-PDT CIGSe absorbers were calculated from the [S]/([S]+[O]) ratios of the Zn(O,S) layers obtained from quantitative XPS analysis. Band gap values for Zn(O,S) layers deposited on the two CIGSe absorbers were estimated as [7]:

$$E_g^{Zn(O,S)} = x \cdot E_g^{ZnS} + (1-x) \cdot E_g^{ZnO} - 3.0 \cdot (1-x) \cdot x \quad (9)$$

where E_g^{ZnS} and E_g^{ZnO} are the band gap values of the end-point materials, which are 3.6 eV and 3.2 eV, respectively [7].

The ΔE_{CBO} values were calculated using the above calculated band gap values and ΔE_{VBO} values (in Table 5) shown in Table 6.

Table 6 CBO calculation of the Na-SLG CIGSe/Zn(O,S) and Na-PDT CIGSe/Zn(O,S) interfaces.

Sample	**GGI**	**CGI**	**E_g^{CIGSe} (eV)**	**SSO**	**$E_g^{Zn(O,S)}$(eV)**	**ΔE_{VBO}(eV)**	**ΔE_{CBO}(eV)**
Na-SLG CIGSe/Zn(O,S)	0.06±0.01	0.26±0.02	1.24±0.06	0.35±0.04	2.66±0.13	-0.93±0.08	0.49±0.16
Na-PDT CIGSe/Zn(O,S)	0.07±0.01	0.26±0.03	1.24±0.06	0.35±0.04	2.66±0.13	-1.20±0.09	0.22±0.17

With the VBO and CBO values established, band diagrams were then constructed for the bare Na-SLG CIGSe and Na-PDT CIGSe absorbers (shown in Figure 6 (a)) and the subsequent Zn(O,S) depositions (shown in Figure 6 (b)). For the beginning, the bulk of both absorbers has been assumed to be purely p-type, i.e. VBM values of 0.25 (net shallow acceptor density, $N_D \sim 10^{16}$ cm^{-3} [45]) have been considered for

both absorbers (Figure 6 (a)). The VBM value being 0.87±0.04 eV and 0.48±0.05 eV for Na-SLG CIGSe and Na-PDT CIGSe surfaces, respectively, the band-bending at the surface is 0.62±0.04 eV and 0.23±0.05 eV for Na-SLG CIGSe and Na-PDT CIGSe, respectively. With the deposition of the initial ultra-thin Zn(O,S) layer, a +0.34 eV (444.84 - 444.50 eV from Table 5) further band-bending is introduced (left panel of Figure 6 (b)) with net band-bending being 0.96 eV at the Na-SLG CIGSe/Zn(O,S) interface and a +0.17 eV (444.73 – 444.56 eV from Table 5) further band-bending is introduced (right panel of Figure 6 (b)) with net band-bending being 0.40±0.05 eV at the Na-PDT CIGSe/Zn(O,S) interface. The deposition of the final thick Zn(O,S) layers establishes the band-alignment of the Zn(O,S) layers with the CIGSe absorbers using the calculated ΔE_{VBO} and ΔE_{CBO} values.

It is known that a few important parameters from the interfacial band-alignment picture can be used to predict device performances in the interfacial recombination regime [47]: (i) the CBO that determines the type of CB alignment; either spike-like ($\Delta E_{CBO}>0$), cliff-like ($\Delta E_{CBO}<0$) or flat-band ($\Delta E_{CBO}=0$), which influences the electron transport through the interface, (ii) the charge carrier cross-recombination barrier height (energy difference between CB of buffer layer and VB of absorber at the interface) which directly influences the open-circuit voltage (V_{oc}) of a device, (iii) type inversion (CB of absorber close to E_F at the interface) or band-bending.

From the band-diagram of Figure 6 (a), it is observed in Na-SLG CIGSe, a type-inverted (p → n) surface is formed (band-bending is greater than or equal to half the band gap). Also, it is seen that the point of midgap (POM), where E_F lies in the middle of the bandgap, is shifted into the absorber (Figure 6 (b)). This indicates Fermi level pinning at the interface. This could be attributed to the presence of positively charged states at the Na-SLG CIGSe surface. This is in accordance with the heterojunction electronic model [43] how larger density of interface states pins E_F at the absorber/buffer interface. The recombination probability in the presence of a high defect density at the interface depends on the product of electron (*n*) and hole concentration (*p*) and is maximum for *n=p*, i.e., at the POM [48]. This way, separating the metallurgical *p-n* junction from the absorber/buffer interface should significantly reduce recombination losses. On the other hand, in case of Na-PDT CIGSe the passivated states (the $(Na_xCu_{1-x})(In_yO_z)$ complex formation) may be pre-dominant over the positively charged surface states and hence in this case the Fermi level is not pinned. The charge carrier cross-recombination barrier height at the Na-SLG CIGSe/Zn(O,S) interface is also larger than that at the Na-PDT CIGSe/Zn(O,S) interface which are 1.73 eV and 1.46 eV (Figure 6 (b)), respectively.

From the band-alignment diagrams of Figure 6 (b), it is found that ΔE_{CBO} is positive for both Na-SLG CIGSe/Zn(O,S) and Na-PDT CIGSe/Zn(O,S) interfaces, i.e. spike-like CBO but being 0.27 eV lesser in the

case of the Na-PDT CIGSe/Zn(O,S) interface. Minemoto et al. [45] showed the influence of the CBO of a CIGSe/ZnO interface on device parameters by numerical calculations. In their device simulations, they vary the CBO from -0.7 to 0.6 eV. In the spike-like or positive CBO regime, their results show constant and high values of all cell parameters as long as CBO is 0.4 eV and below. Above 0.4 eV CBO, both the short-circuit current density (J_{sc}) and the fill factor (FF) decrease abruptly and with that the efficiencies (η). Therefore, the limiting barrier height seen by photo-generated electrons in the absorber is 0.4 eV. Thus, the higher ΔE_{CBO} at the Na-SLG CIGSe/Zn(O,S) interface could have a significant detrimental influence on the V_{oc} of the device.

4. Conclusions

In this work, a systematic analysis of the differences in Na from the SLG substrate (Na-SLG) and Na from a post-deposition treatment (Na-PDT), as per their surface chemical and electronic effects on CIGSe, has been done.

The origin of the shifts in the various experimental XPS peak components observed in the case of Na-SLG CIGSe and Na-PDT CIGSe surfaces have been interpreted in terms of initial and final state contributions to the BE shifts w.r.t. the metallic states as well as with the aid of reference surfaces of Na-PDT (Si) and Na-free CIGSe. Na as post-deposition brings about a Cu-depletion and In_yO_z formation at the CIGSe surface. Furthermore, Na replacing Cu indicates towards formation of a Na-containing complex of the form $(Na_xCu_{1-x})(In_yO_z)$. On the other hand, no chemical interaction of Na in Na-SLG with any of the CIGSe-related components has been found. In this work, we have shown how an Auger parameter analysis of the XPS data can be utilized to determine chemical states of elements. By separating initial and final state effects, it was possible to associate different Na components to different possible surface species in a complex material like CIGSe, which has not been done before. This kind of detailed surface analysis approach can be applied to studies involving CIGSe subject to other alkali PDT (K, Rb, Cs).

Band-alignment studies of the Na-SLG CIGSe and Na-PDT CIGSe surfaces with Zn(O,S) overlayer helped in providing insight into the electronic structure of the heterointerface in both cases and revealed some significant differences in the band-offsets. A greater VBM and interface-induced band-bending induces a type-inversion at the Na-SLG CIGSe/Zn(O,S) interface, which can reduce greatly reduce recombination losses at the interface. The CBO is slightly enhanced to more than the limiting value of 0.4 eV, which may possibly lead to a degraded cell performance. On the other hand, the Na-PDT CIGSe/Zn(O,S) interface has a near optimal CBO value that could lead to a good working solar cell device. However, a Na-containing complex formation at the absorber surface hinders the occurrence of an interfacial type-inversion and a

reduced VBM increases possibility of interface recombination. In general, it is clear that the presence of a surface compound formation is not desirable if it cannot improve the heterojunction, which is the case here. But in spite of a surface species formation, other factors like an optimum CBO may compensate for the absence of a type-inversion provided that the major recombination losses are not from the absorber bulk.

Acknowledgements

I. M. thanks her doctoral funding agencies Erasmus Mundus, FAZIT Stiftung and HZB PVcomB. I. M. also thanks Prof. P. Fumagalli and Dr. R. Püttner (FU Berlin, FB Physik) for error considerations and Auger spectra analysis related discussions.

Figure captions

Figure 1 (color online) (a) Na $1s_{1/2}$ photoelectron and **(b)** Na $KL_{23}L_{23}$ Auger XPS signals from Na-SLG CIGSe, Na-PDT CIGSe and Na-PDT (Si). The Na $KL_{23}L_{23}$ peak contributions are shown in Table 1.

Figure 2 (color online) Wagner plot for sodium. Core-level BE, Auger line KE values of compounds from literature (black) were taken from [49].

Figure 3 (color online) Initial ($\Delta(V_{MA}+kq_A)$) and final state ($-\Delta R^{ea}{}_A$) effects separation in the Auger parameter shifts.

Figure 4 (color online) In $M_{4,5}N_{45}N_{45}$ Auger emission signals from Na-free CIGSe, Na-SLG CIGSe and Na-PDT CIGSe. Closed circles represent raw data and open circles represent the overall envelope of the spectra. Inset 4 (a) and (b) show the normalized intensities of the In $M_5N_{45}N_{45}$ and In $M_4N_{45}N_{45}$ regions, respectively, in detail to show the differences in peak shape.

Figure 5 (color online) UPS spectra of the valence band region probed for the Na-SLG (in red) and Na-PDT (in blue) CIGSe absorbers. Inset shows the valence band region probed for the reference Na-free (in black) CIGSe absorber surface.

Figure 6 (color online) (a) Band-bending at the Na-SLG CIGSe and Na-PDT CIGSe absorber surfaces; **(b)** Band-alignment of the absorber surfaces with Zn(O,S) buffer layer. All energy values shown are in eVs.

Figures

Figure 1

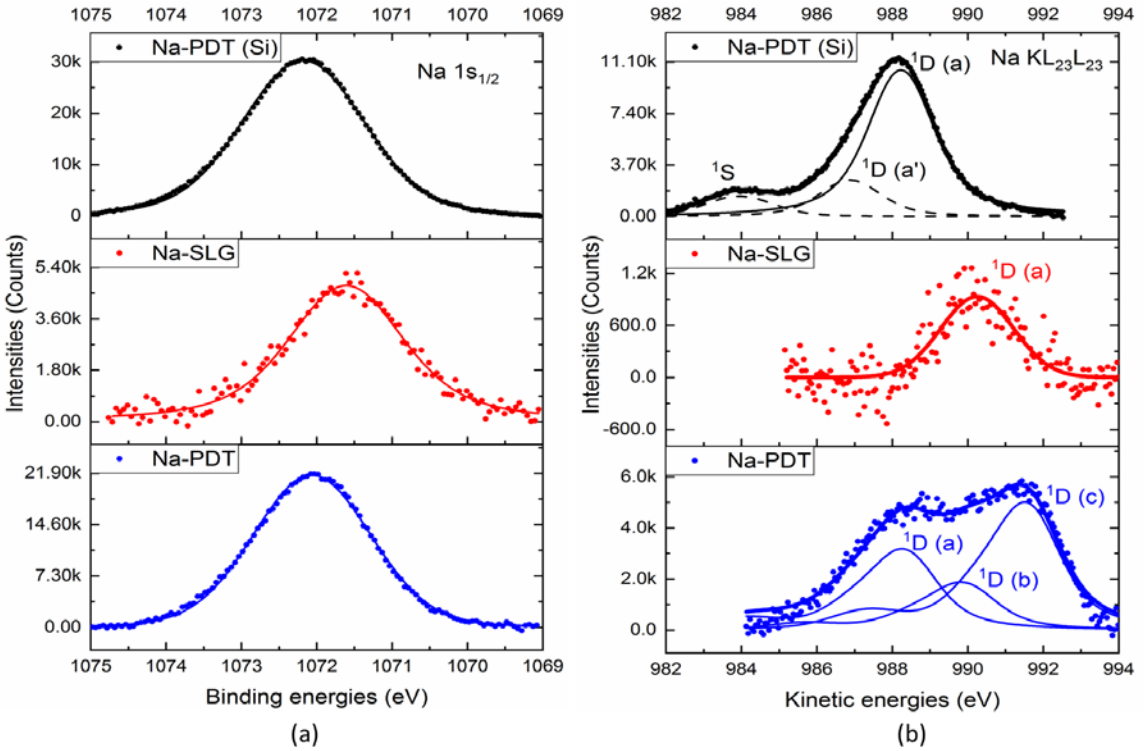
Na-PDT (Si)
Na 1s1/2
Na-SLG
Na-PDT
Intensities (Counts)
Binding energies (eV)
(a)
Na-PDT (Si)
1D (a)
Na KL23L23
1S
1D (a')
Na-SLG
1D (a)
Na-PDT
1D (c)
1D (a)
1D (b)
Kinetic energies (eV)
(b)

Figure 2

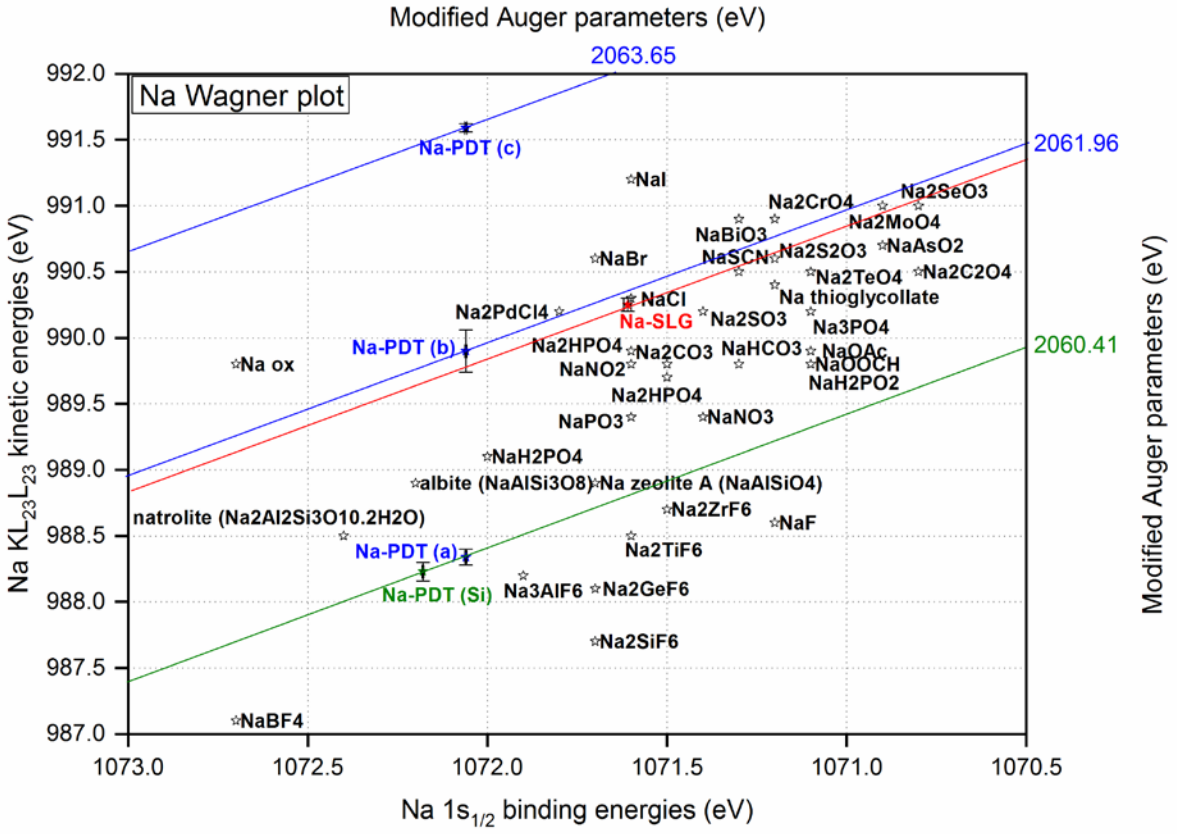

Figure 3

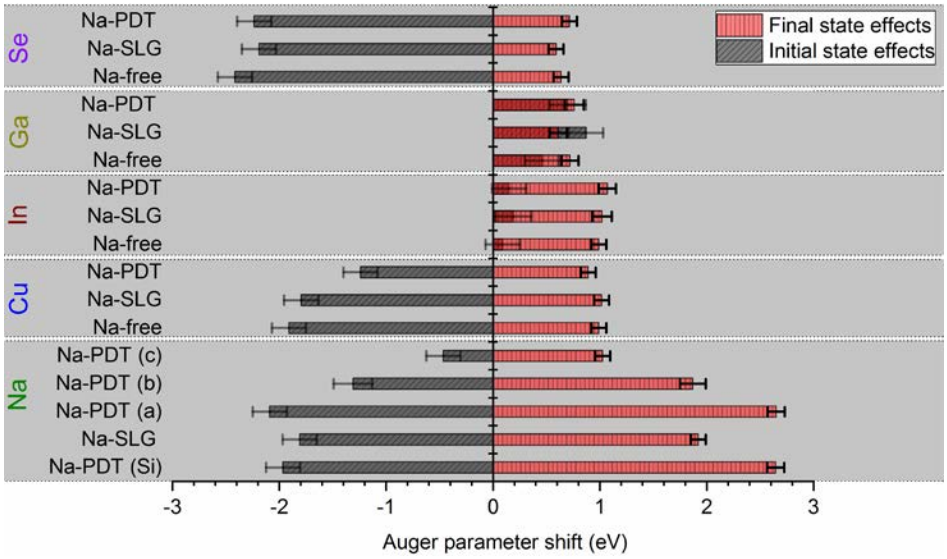

Figure 4

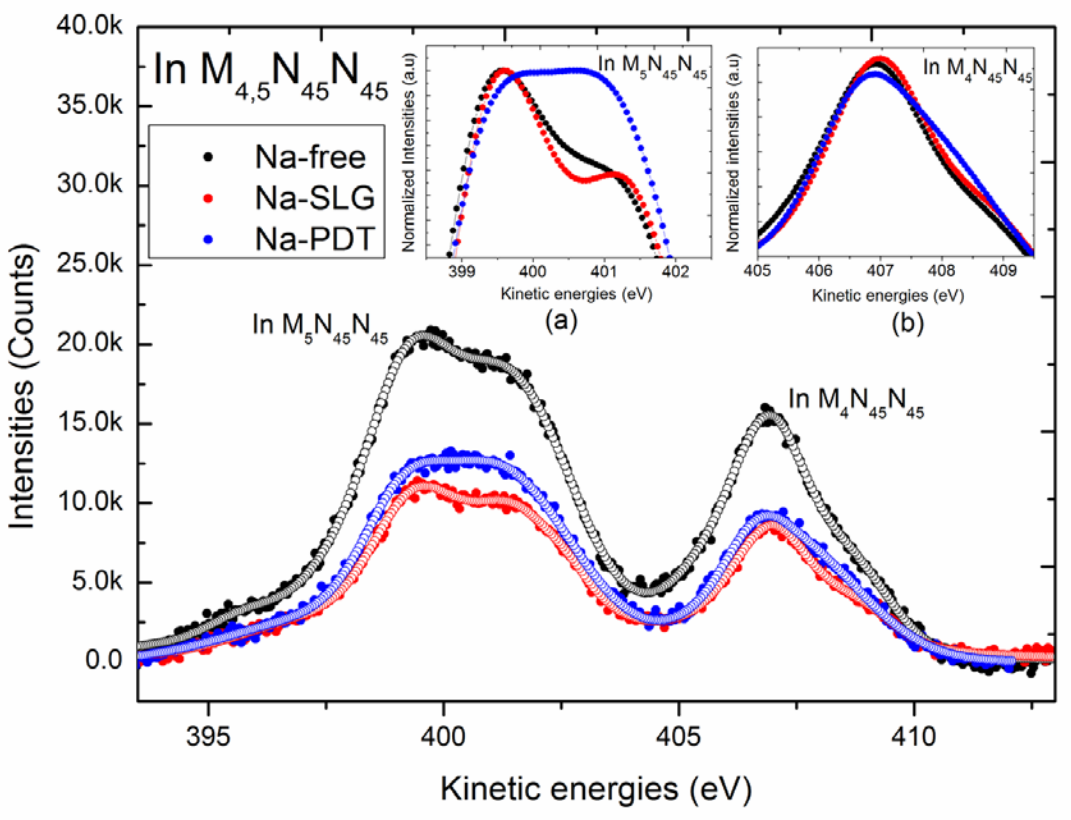

Figure 5

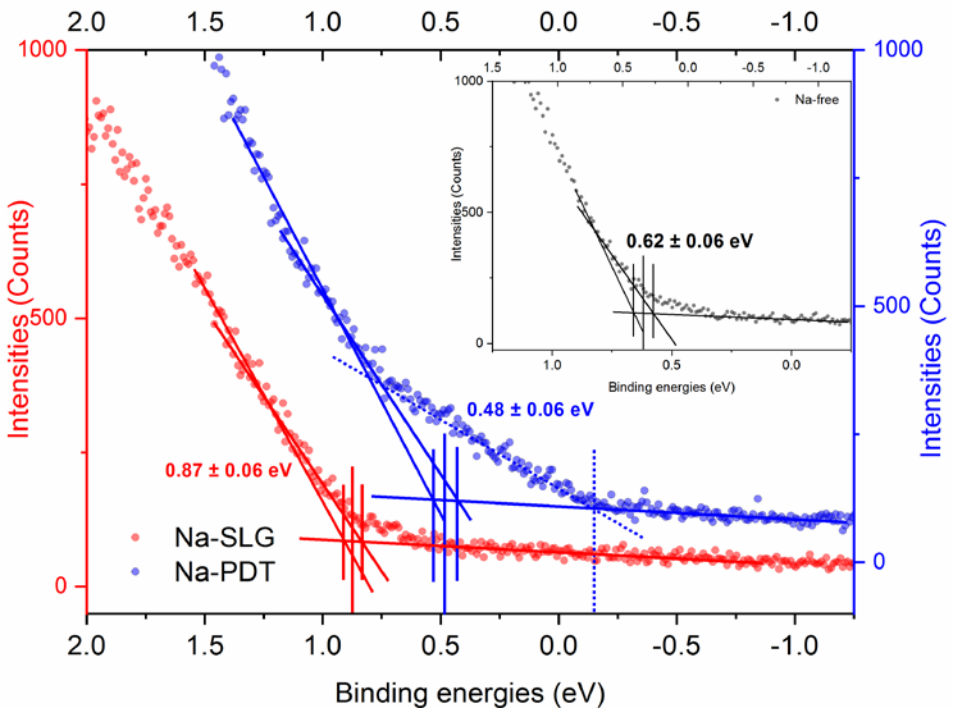

Figure 6

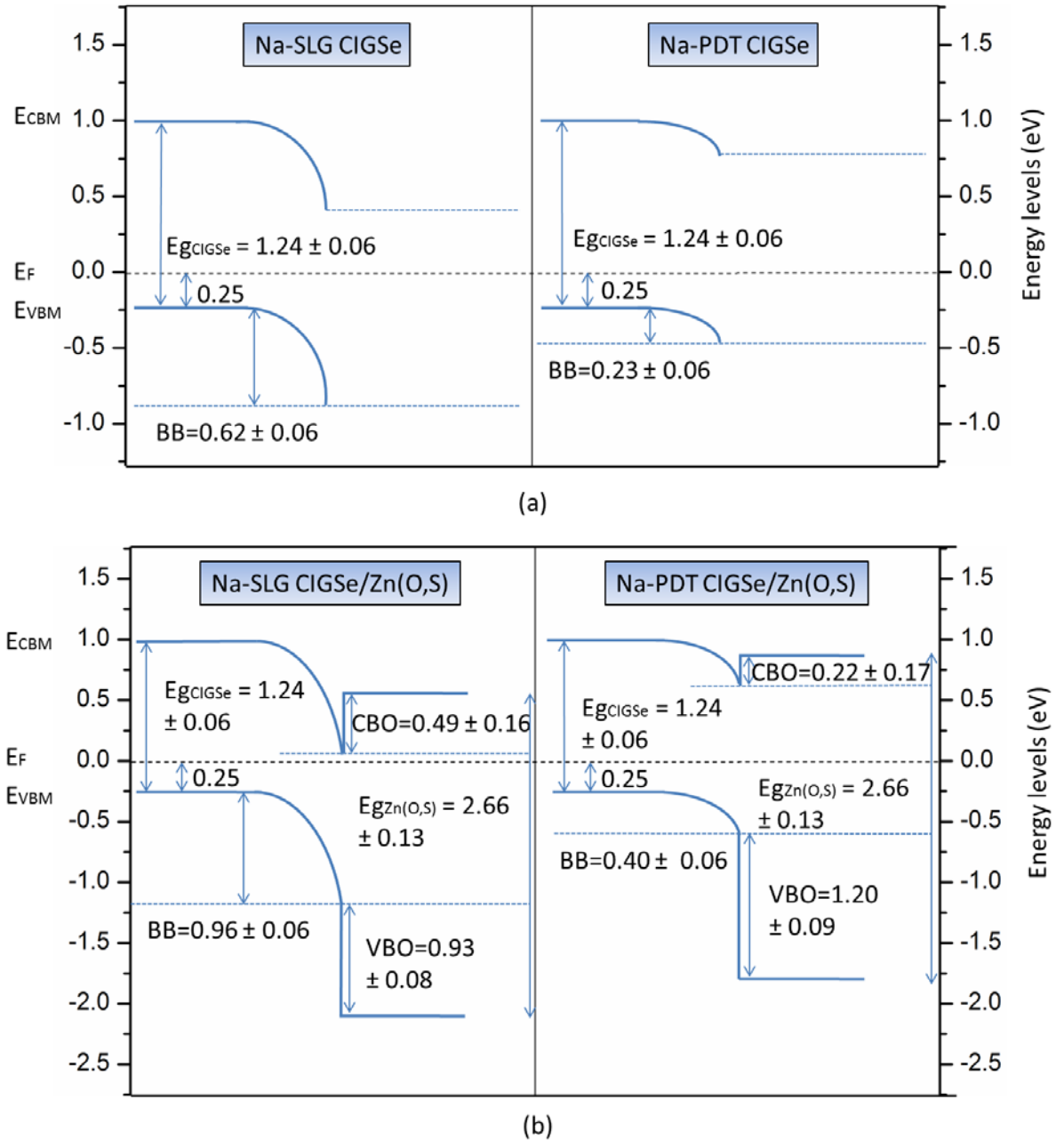

References

[1] J. Hedstrom, H. Ohlsen, M. Bodegard, A. Kylner, L. Stolt, D. Hariskos, M. Ruckh, H.W. Schock, Zno/Cds/Cu(in,Ga)Se2 Thin-Film Solar-Cells with Improved Performance, Ieee Phot Spec Conf, DOI Doi 10.1109/Pvsc.1993.347154(1993) 364-371.

[2] J. Holz, Karg, F., von Philipsborn, H., The effect of substrate impurities on the eletcronic conductivity in CIS thin films, 12th European Photovoltaic Solar Energy Conference, Amsterdam, The Netherlands, DOI (1994) 1592.
[3] P.M.P. Salome, H. Rodriguez-Alvarez, S. Sadewasser, Incorporation of alkali metals in chalcogenide solar cells, Sol Energ Mat Sol C, 143 (2015) 9-20.
[4] D. Rudmann, A.F. da Cunha, M. Kaelin, F. Kurdesau, H. Zogg, A.N. Tiwari, G. Bilger, Efficiency enhancement of Cu(In,Ga)Se_2 solar cells due to post-deposition Na incorporation, Appl Phys Lett, 84 (2004) 1129-1131.
[5] D. Rudmann, D. Bremaud, A.F. da Cunha, G. Bilger, A. Strohm, M. Kaelin, H. Zogg, A. Tiwari, Sodium incorporation strategies for CIGS growth at different temperatures, Thin Solid Films, 480 (2005) 55-60.
[6] M. Lammer, U. Klemm, M. Powalla, Sodium co-evaporation for low temperature Cu(In,Ga)Se-2 deposition, Thin Solid Films, 387 (2001) 33-36.
[7] A. Grimm, D. Kieven, R. Klenk, I. Lauermann, A. Neisser, T. Niesen, J. Palm, Junction formation in chalcopyrite solar cells by sputtered wide gap compound semiconductors, Thin Solid Films, 520 (2011) 1330-1333.
[8] D. Kieven, A. Grimm, I. Lauermann, M.C. Lux-Steiner, J. Palm, T. Niesen, R. Klenk, Band alignment at sputtered ZnSxO1-x/Cu(In,Ga)(Se,S)(2) heterojunctions, Phys Status Solidi-R, 6 (2012) 294-296.
[9] J.W. Pankow, K.X. Steirer, L.M. Mansfield, R.L. Garris, K. Ramanathan, G.R. Teeter, Band alignment of CBD deposited Zn(O,S)/Cu(In1-xGax)Se-2 interface, 2014 Ieee 40th Photovoltaic Specialist Conference (Pvsc), DOI (2014) 1670-1673.
[10] D.R. Scherer, D.B. Fenner, J.M. Hensley, Characterization of alkali metal dispensers and non-evaporable getter pumps in ultrahigh vacuum systems for cold atomic sensors, J Vac Sci Technol A, 30 (2012).
[11] Automated peak separation and analysis PeakFit Version 4.11, http://www.sigmaplot.co.uk/products/peakfit/peakfit4_12_brochure.pdf, DOI.
[12] M.P. Seah, Post-1989 Calibration Energies for X-Ray Photoelectron Spectrometers and the 1990 Josephson Constant, Surf Interface Anal, 14 (1989) 488-488.
[13] R. Klenk, A. Steigert, T. Rissom, D. Greiner, C.A. Kaufmann, T. Unold, M.C. Lux-Steiner, Junction formation by Zn(O, S) sputtering yields CIGSe-based cells with efficiencies exceeding 18%, Prog Photovoltaics, 22 (2014) 161-165.
[14] H. Hillig, B. Cleff, W. Mehlhorn, W. Schmitz, K-Auger Transitions of Free Sodium Atom, Z Phys, 268 (1974) 225-233.

[15] A. Barrie, F.J. Street, Auger and X-Ray Photoelectron Spectroscopic Study of Sodium Metal and Sodium Oxide, J Electron Spectrosc, 7 (1975) 1-31.
[16] P. Steiner, F.J. Reiter, H. Hochst, S. Hufner, Kll Auger-Spectra of Na and Mg Metal and Their Plasmon Structure, Phys Status Solidi B, 90 (1978) 45-51.
[17] D. Rudmann, Effects of sodium on growth and properties of Cu(In,Ga)Se_2 thin films and solar cells, PhD Dissertation, Swiss Federal Institute of Technology (ETH), Zürich, DOI (2004).
[18] J.H. Yoon, T.Y. Seong, J.H. Jeong, Effect of a Mo back contact on Na diffusion in CIGS thin film solar cells, Prog Photovoltaics, 21 (2013) 58-63.
[19] K. Sakurai, A. Yamada, P. Fons, K. Matsubara, T. Kojima, S. Niki, T. Baba, N. Tsuchimochi, Y. Kimura, H. Nakanishi, Adjusting the sodium diffusion into CuInGaSe2 absorbers by preheating of Mo/SLG substrates, J Phys Chem Solids, 64 (2003) 1877-1880.
[20] V. Probst, F. Karg, J. Rimmasch, W. Riedl, W. Stetter, H. Harms, O. Eibl, Advanced stacked elemental layer process for Cu(InGa)Se-2 thin film photovoltaic devices, Mater Res Soc Symp P, 426 (1996) 165-176.
[21] D. Braunger, D. Hariskos, G. Bilger, U. Rau, H.W. Schock, Influence of sodium on the growth of polycrystalline Cu(In,Ga)Se(2) thin films, Thin Solid Films, 361 (2000) 161-166.
[22] R.V. Forest, Diffusion of Na in copper indium gallium diselenide based materials, PhD Dissertation, University of Delaware, DOI (2015).
[23] W. Calvet, Majumdar, I., Ümsür, B., Steigert, A., Chacko, B., Parvan, V., Olar, T.,Kaufmann, C. A., Greiner, D., Lauche, J., Navirian, H., Voorwinden, G., Mannstadt, W., Schlatmann, R., Lux-Steiner, M. Ch., Lauermann, I., Analysis of surface composition and device performance of UHV and air-transferred CIGSe thin film solar cell absorbers on alkali-containing substrate glass, 32nd European Photovoltaic Solar Energy Conference (EUPVSEC), Munich, Germany, DOI (2016).
[24] X. Song, R. Caballero, R. Felix, D. Gerlach, C.A. Kaufmann, H.W. Schock, R.G. Wilks, M. Bar, Na incorporation into Cu(ln,Ga)Se-2 thin-film solar cell absorbers deposited on polyimide: Impact on the chemical and electronic surface structure, Journal of Applied Physics, 111 (2012).
[25] M.J. Guittet, J.P. Crocombette, M. Gautier-Soyer, Bonding and XPS chemical shifts in ZrSiO4 versus SiO2 and ZrO2: Charge transfer and electrostatic effects, Phys Rev B, 63 (2001).
[26] C.D. Wagner, Chemical-Shifts of Auger Lines, and Auger Parameter, Faraday Discussions, 60 (1975) 291-300.
[27] T.D. Thomas, Extra-Atomic Relaxation Energies and the Auger Parameter, Journal of Electron Spectroscopy and Related Phenomena, 20 (1980) 117-125.
[28] G. Moretti, Auger parameter and Wagner plot in the characterization of chemical states by X-ray photoelectron spectroscopy: a review, J Electron Spectrosc, 95 (1998) 95-144.

[29] M. Satta, G. Moretti, Auger parameters and Wagner plots, J Electron Spectrosc, 178 (2010) 123-127.
[30] Kowalczy.Sp, L. Ley, F.R. Mcfeely, R.A. Pollak, D.A. Shirley, X-Ray Photoemission from Sodium and Lithium, Phys Rev B, 8 (1973) 3583-3585.
[31] J.C. Fuggle, E. Kallne, L.M. Watson, D.J. Fabian, Electronic-Structure of Aluminum and Aluminum-Noble-Metal Alloys Studied by Soft-X-Ray and X-Ray Photoelectron Spectroscopies, Phys Rev B, 16 (1977) 750-761.
[32] G.D. Nichols, D.A. Zatko, Photoelectron and Auger-Spectroscopy of Indium Halides, Oxide and Sulfide Compounds, Inorg Nucl Chem Lett, 15 (1979) 401-404.
[33] G. Schön, Auger and direct electron spectra in X-ray photoelectron studies of zinc, zinc oxide, gallium and gallium oxide, J Electron Spectrosc, 2 (1973) 75-86.
[34] C.D. Wagner, L.H. Gale, R.H. Raymond, 2-Dimensional Chemical-State Plots - Standardized Data Set for Use in Identifying Chemical-States by X-Ray Photoelectron-Spectroscopy, Anal Chem, 51 (1979) 466-482.
[35] E.J. Aitken, M.K. Bahl, K.D. Bomben, J.K. Gimzewski, G.S. Nolan, T.D. Thomas, Electron Spectroscopic Investigations of the Influence of Initial-State and Final-State Effects on Electronegativity, J Am Chem Soc, 102 (1980) 4873-4879.
[36] O. Cojocaru-Miredin, P. Choi, R. Wuerz, D. Raabe, Exploring the p-n junction region in Cu(In,Ga)Se-2 thin-film solar cells at the nanometer-scale, Appl Phys Lett, 101 (2012).
[37] C. Heske, G. Richter, Z.H. Chen, R. Fink, E. Umbach, W. Riedl, F. Karg, Influence of Na and H2O on the surface properties of Cu(In,Ga)Se, thin films, Journal of Applied Physics, 82 (1997) 2411-2420.
[38] V. Parvan, A. Mizrak, I. Majumdar, B. Umsur, W. Calvet, D. Greiner, C.A. Kaufmann, T. Dittrich, E. Avancini, I. Lauermann, Cu(In, Ga)Se-2 surface treatment with Na and NaF: A combined photoelectron spectroscopy and surface photovoltage study in ultra-high vacuum, Appl Surf Sci, 444 (2018) 436-441.
[39] M.B. Trzhaskovskaya, V.I. Nefedov, V.G. Yarzhemsky, Photoelectron angular distribution parameters for elements Z=1 to Z=54 in the photoelectron energy range 100-5000 eV, Atom Data Nucl Data, 77 (2001) 97-159.
[40] M. Malitckaya, H.P. Komsa, V. Havu, M.J. Puska, Effect of Alkali Metal Atom Doping on the CuInSe2-Based Solar Cell Absorber, J Phys Chem C, 121 (2017) 15516-15528.
[41] S.H. Wei, S.B. Zhang, A. Zunger, Effects of Na on the electrical and structural properties of CuInSe2, Journal of Applied Physics, 85 (1999) 7214-7218.
[42] A.D. Katnani, G. Margaritondo, Microscopic Study of Semiconductor Heterojunctions - Photoemission Measurement of the Valance-Band Discontinuity and of the Potential Barriers, Phys Rev B, 28 (1983) 1944-1956.

[43] U. Rau, D. Braunger, R. Herberholz, H.W. Schock, J.F. Guillemoles, L. Kronik, D. Cahen, Oxygenation and air-annealing effects on the electronic properties of Cu(In,Ga)Se-2 films and devices, Journal of Applied Physics, 86 (1999) 497-505.
[44] M.A. Contreras, Wiesner, H., Niles, D., Ramanathan, K., Matson, R., Tuttle, J., Keane, J., Noufi, R., Defect Chalcopyrite $Cu(In_{1-x}Ga_x)_3Se_5$ Materials and High-Ga-Content $Cu(In,Ga)Se_2$-based Solar Cells, IEEE 25th Photovoltaic Specialist Conference (PVSC) DOI (1996) 809-812.
[45] T. Minemoto, T. Matsui, H. Takakura, Y. Hamakawa, T. Negami, Y. Hashimoto, T. Uenoyama, M. Kitagawa, Theoretical analysis of the effect of conduction band offset of window/CIS layers on performance of CIS solar cells using device simulation, Sol Energ Mat Sol C, 67 (2001) 83-88.
[46] D. Kuciauskas, J.V. Li, M.A. Contreras, J. Pankow, P. Dippo, M. Young, L.M. Mansfield, R. Noufi, D. Levi, Charge carrier dynamics and recombination in graded band gap CuIn1-xGaxSe2 polycrystalline thin-film photovoltaic solar cell absorbers, Journal of Applied Physics, 114 (2013).
[47] R. Klenk, Characterisation and modelling of chalcopyrite solar cells, Thin Solid Films, 387 (2001) 135-140.
[48] P.a.K. Pistor, R. , On the advantage of a buried pn-junction in chalcopyrite solar cells: An urban legend?, Proceedings of NUMOS, Gent, 28-30 March 2007, DOI (2007) 179-182.
[49] M.P.S. D. Briggs, Practical Surface Analysis by Auger and X-ray Photoelectron Spectroscopy, DOI (1983).